



The effect of 3D hydrogel scaffold modulus on osteoblast differentiation and mineralization revealed by combinatorial screening

Kaushik Chatterjee^{a,b}, Sheng Lin-Gibson^a, William E. Wallace^a, Sapun H. Parekh^a, Young Jong Lee^a, Marcus T. Cicerone^a, Marian F. Young^b, Carl G. Simon Jr.^{a,*}

^a Polymers Division, National Institute of Standards and Technology, Gaithersburg, MD, USA

^b Craniofacial and Skeletal Diseases Branch, National Institute of Dental and Craniofacial Research, National Institutes of Health, Bethesda, MD, USA

ARTICLE INFO

Article history:

Received 14 January 2010

Accepted 9 March 2010

Available online 7 April 2010

Keywords:

Tissue engineering

Hydrogels

Osteoblast

Combinatorial methods

Matrix stiffness

Graded tissues

ABSTRACT

Cells are known to sense and respond to the physical properties of their environment and those of tissue scaffolds. Optimizing these cell–material interactions is critical in tissue engineering. In this work, a simple and inexpensive combinatorial platform was developed to rapidly screen three-dimensional (3D) tissue scaffolds and was applied to screen the effect of scaffold properties for tissue engineering of bone. Differentiation of osteoblasts was examined in poly(ethylene glycol) hydrogel gradients spanning a 30-fold range in compressive modulus (≈ 10 kPa to ≈ 300 kPa). Results demonstrate that material properties (gel stiffness) of scaffolds can be leveraged to induce cell differentiation in 3D culture as an alternative to biochemical cues such as soluble supplements, immobilized biomolecules and vectors, which are often expensive, labile and potentially carcinogenic. Gel moduli of ≈ 225 kPa and higher enhanced osteogenesis. Furthermore, it is proposed that material-induced cell differentiation can be modulated to engineer seamless tissue interfaces between mineralized bone tissue and softer tissues such as ligaments and tendons. This work presents a combinatorial method to screen biological response to 3D hydrogel scaffolds that more closely mimics the 3D environment experienced by cells in vivo.

Published by Elsevier Ltd.

1. Introduction

Regenerative medicine offers hope to millions of patients suffering from a wide variety of debilitating diseases. Engineered tissues and organs can bridge the ever-increasing gap between the demand and availability of donor organs [1]. Over the past decade, billions of dollars have been invested in the development of tissue-engineered products and yet the industry is only just beginning to become profitable [2]. A key challenge in this field is identifying optimal scaffold properties that promote desired tissue regeneration [1].

Combinatorial methods applied successfully by the pharmaceuticals industry for drug discovery are being adapted towards accelerating the pace of tissue engineering research [3–10]. These methods have typically utilized two-dimensional (2D) culture formats where cells were cultured on material surfaces. However, it has become well-accepted that cells cultured in a three-dimensional (3D) environment behave more like cells in native tissue than those cultured in 2D formats [11]. The objective of this work was to develop a simple combinatorial technique to enable rapid screening of 3D tissue scaffolds. The combinatorial platform was

applied herein to systematically screen the effect of mechanical properties of poly(ethylene glycol) dimethacrylate (PEGDM) hydrogels on differentiation of encapsulated osteoblasts.

Photopolymerizable poly(ethylene glycol) (PEG) hydrogels have emerged as promising 3D scaffolds for tissue engineering [12–17]. They have the advantage of being injectable for curing in situ [13]. Though the effects of PEG-based hydrogel chemical/physical properties (functionality, stiffness, and degradation) and biological properties (release of soluble proteins and growth factors, presence of cross-linked peptides or other bioactive moieties) on cell response have been demonstrated [12–17], these parameters have not been optimized to maximize tissue regeneration in 3D.

The fabrication approach utilized in this work yielded hydrogel scaffold gradients containing a 30-fold range (≈ 10 kPa to ≈ 300 kPa) in compressive modulus variation and contained osteoblasts in situ. The MC3T3-E1 murine cell line, a classic osteoblast model, was used to study differentiation and mineralization after encapsulation in hydrogel gradients. The results herein demonstrate that scaffold stiffness can be used to direct osteogenesis in 3D culture towards generation of mineralized tissue.

In addition, the hydrogel modulus gradients induced formation of mineralized tissue gradients. Gradients are prevalent in biology, and gradients in molecules, composition and properties exist at the

* Corresponding author. Tel.: +1 301 975 8574; fax: +1 301 975 4977.

E-mail address: carl.simon@nist.gov (C.G. Simon Jr.).

interfacial regions of many tissues such as ligaments [18], teeth [19] and intestine [20]. During organismal development, morphogen gradients are a primary mechanism used to drive pattern formation and organogenesis [21]. Thus, approaches for engineering graded tissues are critical in regenerative medicine. The mineralization gradients presented herein are unique because they were fabricated from a single material (PEGDM), did not require the addition of osteogenic supplements, were fabricated with osteoblasts *in situ*, were induced by varying only a material property (compressive modulus) and did not require expensive, labile or potentially carcinogenic factors (peptides, proteins, growth factors, vectors) [22]. Furthermore, mineralization gradients obtained from modulus gradients in this study offer an approach for engineering seamless tissue interfaces for integration of hard and soft tissues as is found in ligaments and tendons.

2. Materials and methods

2.1. Preparation and characterization of poly(ethylene glycol) dimethacrylate

PEGDM was prepared following a previously-reported microwave-assisted reaction [17]. Briefly, PEG (MW = relative molecular mass 4000 g/mol, Sigma–Aldrich) was reacted with 10-fold molar excess of methacrylic anhydride (Sigma–Aldrich) in a standard microwave (GE 1100 W, at maximum power) in five 1 min intervals interspersed with 1 min cooling periods. The solid was dissolved in a minimal volume of methanol (Mallinckrodt Chemicals) and precipitated in excess ether (Sigma–Aldrich) in order to separate unreacted components. The precipitate was collected by vacuum filtration. Approximately 10 g of PEGDM monomer was used for the work described in the current report.

The functionalized product was characterized by matrix-assisted laser desorption/ionization time-of-flight mass spectrometry (MALDI-ToF MS) performed on a Bruker REFLEX II in reflectron mode using two-stage ion extraction [17]. Ablation was performed with a nitrogen gas laser having a 337 nm wavelength. The ion acceleration used was 25 kV. The precipitated product (6 mg) was dissolved in 1 mL of a water:acetonitrile solution (2:1 by volume) with approximately 0.1% by volume of trifluoroacetic acid added. The MALDI matrix, all-trans retinoic acid (5 mg), was dissolved in 1 mL tetrahydrofuran. The cationizing agent, sodium trifluoroacetate (6 mg), was dissolved in 1 mL of the water:acetonitrile solution. These solutions were mixed in a 10:25:10 ratio. This mixture was electrosprayed onto the MALDI target at 5 kV with a flow rate of 5 $\mu\text{L}/\text{min}$ and at distance of approximately 2 cm through a steel needle with an inner diameter of 0.2 mm. The spectrum presented is the sum of 250 discrete laser shots (Fig. 1). The digitization was at 1 ns intervals.

2.2. Cell culture

The MC3T3-E1 cell line was selected to characterize the combinatorial platform because it is a well-characterized murine osteoblast cell line [23] that has been used extensively as a model for osteoblasts yielding a detailed understanding of its behavior *in vitro* [24]. During culture, MC3T3-E1 cells follow well-characterized stages of osteogenesis [25] where they first adhere and proliferate, followed by differentiation and mineralization [26]. Thus, MC3T3-E1 cells are an established model for osteoblasts that can be used to study bone tissue generation *in vitro*.

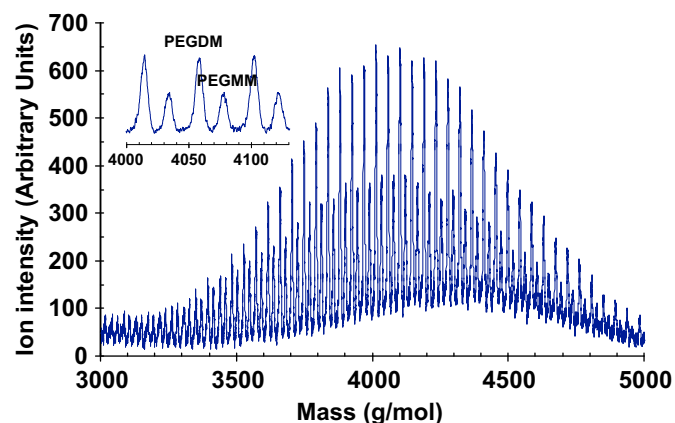


Fig. 1. Full spectra of MALDI-TOF MS of functionalized PEG. Inset shows the expansion of a set of peaks due to the monomethacrylate- (PEGMM) and the dimethacrylate-functionalized (PEGDM) products, respectively.

MC3T3-E1 murine osteoblasts (Riken Cell Bank, Japan) were cultured as described previously [27]. Growth medium was used for all experiments except where indicated. Growth medium was prepared from α -modification of Eagle's minimum essential medium (Invitrogen) supplemented with 10% volume fraction of fetal bovine serum (Gibco) and 0.6% volume fraction of kanamycin sulfate (Sigma–Aldrich). Osteogenic medium was used in a control experiment and consisted of growth medium supplemented with 10 nmol/L dexamethasone (Sigma–Aldrich), 20 mmol/L β -glycerophosphate (Sigma–Aldrich) and 50 $\mu\text{mol}/\text{L}$ L-ascorbic acid 2-phosphate (Sigma–Aldrich). Passage 4 cells were used for all experiments.

2.3. Preparation of gradient hydrogels

The combinatorial platform was assembled using a gradient maker (Hofer SG15, Amersham Biosciences) (Fig. 2) at room temperature (23 °C). The output of the gradient maker was pumped through PVC tubing using a peristaltic pump (MMP-100, C.B.S. Scientific) at 1 mL/min into a single-entry bottom-filling vertical mold (6 cm \times 6 cm \times 3 mm). The mold was prepared by machining a Teflon sheet (10 cm \times 8 cm \times 3 mm) that was tightly clipped between a Teflon block (10 cm \times 8 cm \times 5 mm) and a glass slide (10 cm \times 8 cm \times 1 mm, Amersham Biosciences) so that light could penetrate for photopolymerization. All equipment was sterilized with ethylene oxide and the gradients with encapsulated cells were prepared under aseptic conditions in a cell culture hood.

Pre-polymer solutions were prepared by dissolving 5% and 20% PEGDM mass fractions in phosphate-buffered saline (PBS, Invitrogen) containing 0.05% mass fraction of 1-[4-(2-hydroxyethoxy)-phenyl]-2-hydroxy-2-methyl-1-propane-1-one (Irgacure 2959, Ciba Chemicals). Solutions were sterile filtered (0.22 μm) before suspending 2.5×10^6 cells/mL. To fabricate gradient gels, 5.8 mL of the 5% and 20% PEGDM solutions containing suspended cells were transferred to the mixing and the stock chambers of the gradient maker, respectively. A stir bar was used to mix components in the mixing chamber and turning on the peristaltic pump initiated the gradient fabrication sequence. After the mold was filled (\approx 15 min), the pre-polymer solution was polymerized through the glass slide of the mold by exposure to 2 mW/cm² of 365 nm lamp (UVL-28EL series 8W, UVP) for 15 min.

The cured slab was immediately removed from the mold and cut with a razor along the direction of the gradient into six samples of 6 cm \times 1 cm \times 3 mm. The gels were transferred to 4-well plates with 8 mL culture media and cultured following conditions described above. Gradient gel controls for mechanical characterization and swelling measurements were prepared as described above except that cells were omitted and the gels were incubated in water instead of cell medium. A total of 36 gradients (6 cm \times 1 cm \times 3 mm) were used for the work described: 12 for osteoblast proliferation/differentiation, 6 for osteoblast mineralization and 18 for swelling/modulus measurements. Note that 6 gradients of dimensions (6 cm \times 1 cm \times 3 mm) can be made from each slab gel of dimensions (6 cm \times 6 cm \times 3 mm).

2.4. Preparation of control hydrogels

Control hydrogels of uniform composition were used in many instances to demonstrate that results from gradients could be replicated in uniform samples. Control gels were cylindrical with the following dimensions: 0.05 mL volume, 5 mm diameter, 2.5 mm thick. Controls were made of various compositions with (2.5×10^6 cells/mL) and without cells at room temperature (23 °C) as indicated in the text and figures: 5%, 10%, 15% or 20% by mass of PEGDM. For cell culture experiments, control cylindrical gels with cells were cultured in 48-well plates with 1 mL of medium.

2.5. Viscosity measurements of monomer solutions

Shear viscosity of PEGDM pre-polymer solutions (5%, 10%, or 20% by mass in PBS) was measured using an ARES rheometer (TA Instruments) using a cone-and-plate configuration (diameter = 50 mm, cone angle = 0.04 rad). Viscosity was determined at room temperature (23 °C) over shear rates ranging from 1 s⁻¹–100 s⁻¹, where the viscosity remained constant. Several measurements (between 4 and 8) were made on each solution.

2.6. Mechanical characterization of gradient hydrogels

Compressive modulus of the gels was characterized after the samples were incubated in water for at least 1 d. Each sample was cut orthogonal to the direction of the gradient into six segments of 1 cm \times 1 cm \times 3 mm (Fig. 3b). A circular disk of 8 mm diameter \times 3 mm height was punched from the center of each piece. The disks were subjected to a static compressive axial load at a strain rate of 0.01 mm/s (Enduratec, Bose) at room temperature. The load-displacement data were transformed to stress-strain plots. The slope of a linear fit for 2.5% strain was used as a measure of the compressive modulus. Though most modulus measurements were made at room temperature (23 °C), some control measurements were made at 37 °C. For these measurements, samples were warmed in a 37 °C water bath immediately before making measurements.

To determine the swelling ratio along the gradient, disks were prepared as described above for the compression test. The mass of the disks were measured at equilibrium swelling (1 d). The disks were subsequently dehydrated under vacuum

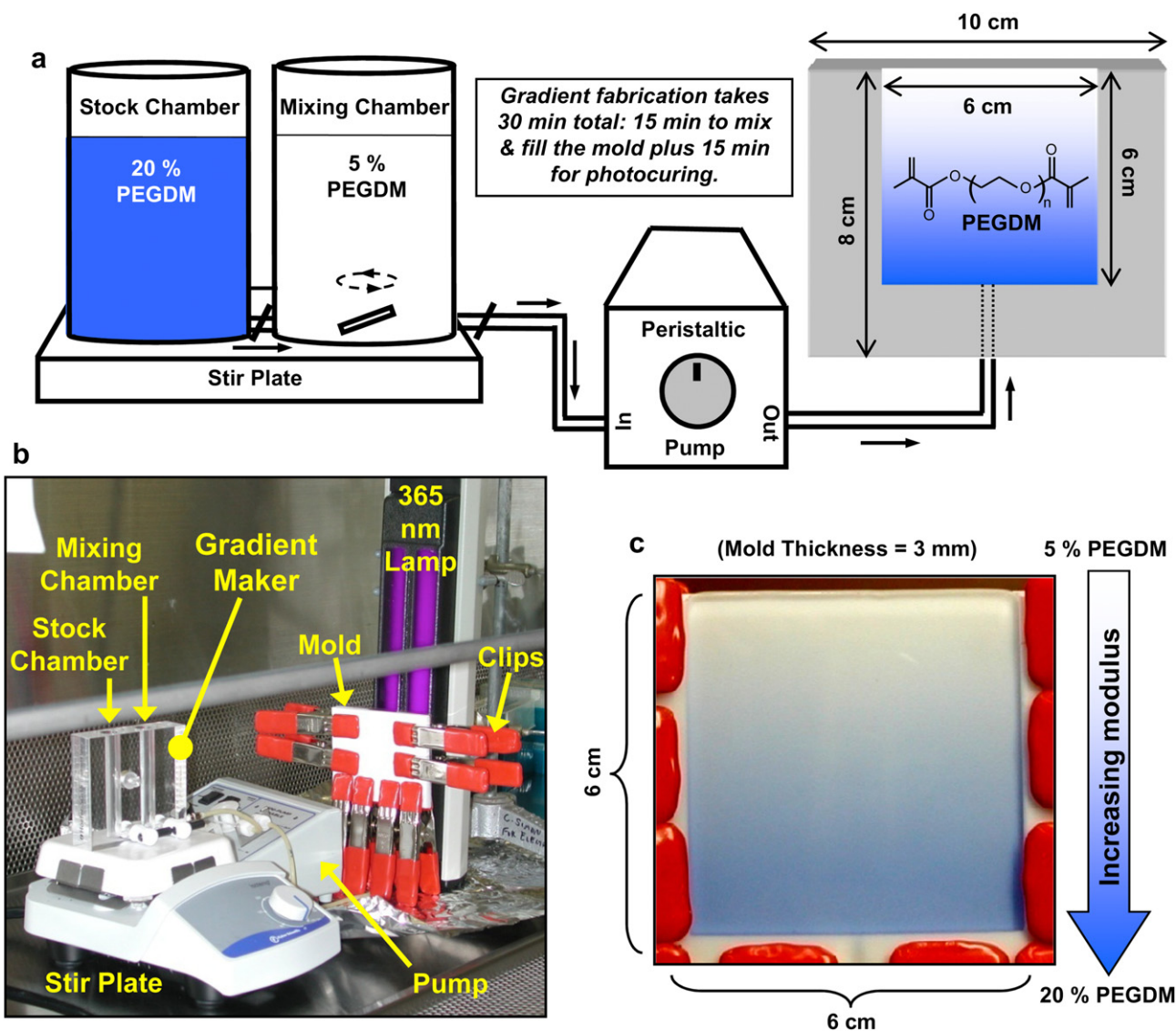


Fig. 2. (a) Schematic illustration of the combinatorial platform used to prepare hydrogel scaffolds with gradients in mechanical stiffness. The output of the gradient maker, placed on a magnetic stir plate, was pumped by a peristaltic pump into a vertical mold and cured with a 365 nm lamp. The structure of PEGDM is shown in the gel gradient on the right. (b) Photograph of the sterilized equipment arranged in a cell culture hood for aseptic gradient fabrication. (c) Image of the mold, as observed through the glass slide, filled with the output of the gradient maker wherein a trace amount of Trypan Blue dye was added to the solution in the stock chamber containing 20% PEGDM. Each mold yielded a square gradient gel (6 cm × 6 cm × 3 mm) which was cut into six gradient slab scaffolds of 6 cm × 1 cm × 3 mm.

for 2 d and the mass of the dry solid was measured again. The swelling ratio equals mass of the swollen gel at equilibrium divided by mass of the dried solid.

2.7. Measurement of cell response in gradients

The effect of hydrogel modulus on the viability and differentiation of encapsulated osteoblasts was assessed at 1 d, 7 d, 21 d and 42 d following scaffold fabrication. At the indicated time points, gradient hydrogel scaffolds were cut orthogonal to the direction of the modulus gradient into six equal segments (Fig. 3b). Each segment was further cut parallel to the direction of the gradient into five equal sections (1 cm × 2 mm × 3 mm) for use in five cell assays. Three measures of cell viability/number and two tests of osteogenic differentiation were used: Live/Dead, Wst-1, Picogreen, alkaline phosphatase and Alizarin Red S. All measurements were performed on three independent samples; there were 3 gradients for each time point ($n = 3$ for all data points).

2.8. Live/dead staining

Live/Dead stain is a vital fluorescence double-stain based on membrane integrity and intracellular esterase activity where micrographs are used to semi-quantitatively assess cell viability. Gel sections were incubated at 37 °C for 30 min in PBS containing 2 μM calcein AM (Live) and 2 μM ethidium homodimer-1 (Dead) (Invitrogen). Cells stained green (live) and red (dead) were imaged using an inverted

epifluorescence microscope (Nikon Eclipse TE 300). Two fields were imaged on both green and red channels and the number of live and dead cells was counted manually for each image. The ratio of number of live cells divided by the sum of the number of live and dead cells was defined as the fractional viability.

2.9. Wst-1 assay

Wst-1 assay was used to measure cellular metabolic dehydrogenase activity in non-homogenized gels (cells must remain intact for the assay). Gel sections containing intact cells were incubated for 3 h in 24-well plates at 37 °C with 1 mL Wst-1 solution [Tyrode's-Hepes buffer containing 45 μmol/L Wst-1 [2-(4-iodophenyl)-3-(4-nitrophenyl)-5-(2,4-disulphophenyl)-2H-tetrazolium, monosodium salt] and 2 μmol/L 1-methoxy-5-methylphenazinium methylsulfate; Dojindo]. Aliquots (0.2 mL) from the reacted solutions were transferred to a 96-well plate and absorbance at 450 nm was measured by a microplate reader (SpectraMax M5, Molecular Dynamics). Wst-1 measurements were normalized to the mass of the gel slices to account for differences in the size of the gel slices.

2.10. Picogreen assay

Picogreen measures detergent-extracted DNA from dounce-homogenized gel specimens. DNA content in the gels was determined using the Picogreen dsDNA Quantitation Kit (Molecular Probes). Gel sections were homogenized manually in

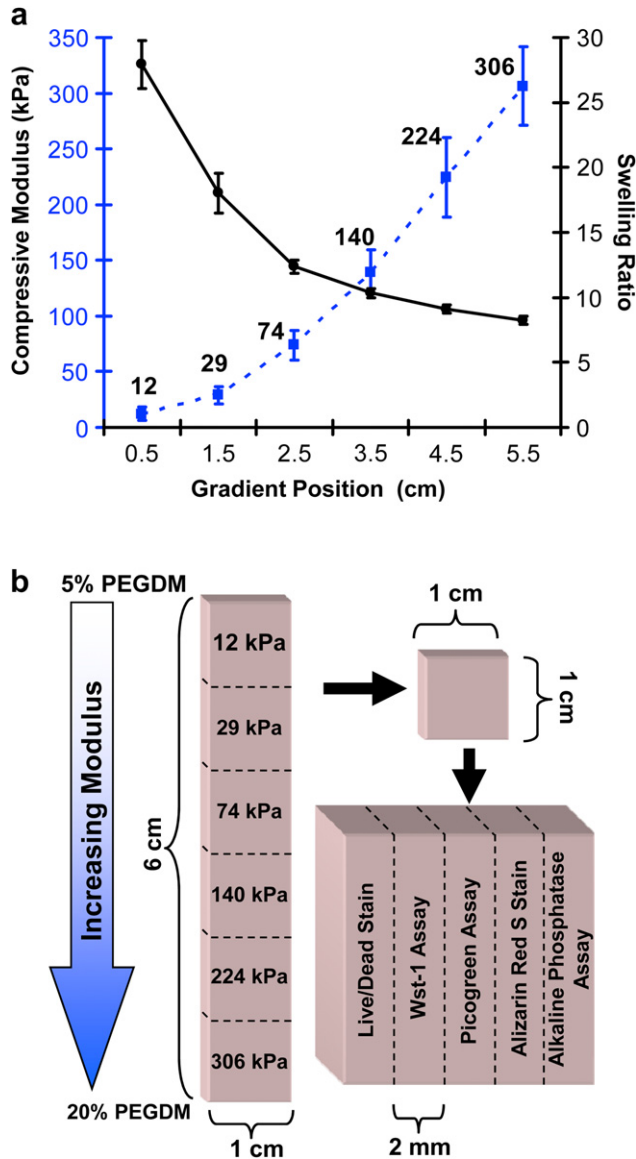


Fig. 3. (a) The compressive modulus (dotted blue line) and swelling ratio (solid black line) are plotted for the gel at different positions along the gradient. Error bars are standard deviation and n is 18 for each data point. Guidelines are drawn to aid the eye. Statistical analyses are presented in Fig. S1. (b) Experimental scheme to characterize the cell response in the gradient hydrogels. Gradients were cut into six segments of 1 cm × 1 cm × 3 mm along the direction of the stiffness gradient. To determine the cellular response the gels were further cut into five equal sections of 1 cm × 2 mm × 3 mm for the five assays and stains indicated. The numbers on the 6 gel sections on the left correspond to modulus.

a tissue grinder (Kontes Glass Company) in a buffer from the kit containing 0.3% by mass sodium dodecyl sulfate (SDS, Sigma–Aldrich) and 0.8 mg/mL Proteinase K (Sigma–Aldrich). Samples were incubated overnight at 37 °C and 0.1 mL of solution was transferred to a 96-well plate with 0.1 mL of Picogreen solution (from kit). Fluorescence intensity was measured by a microplate reader using excitation and emission wavelengths of 488 nm and 525 nm, respectively. DNA concentration is determined by generating a calibration curve using serial dilutions of a DNA control which is provided with the kit. Picogreen DNA measurements were normalized to the mass of the gel slices to account for differences in the size of the gel slices.

2.11. Alkaline phosphatase assay

Alkaline phosphatase expression levels were assessed using Alkaline Phosphatase Detection Reagent (Stanbio Laboratory). Gel sections were incubated at 37 °C in a 24-well plate with 0.5 mL of 1% by mass Nonidet P-40 detergent solution (Roche Diagnostics) for 4 h. An aliquot (0.1 mL) of the reacted solution was transferred to

a 48-well plate and incubated at 22 °C with 0.5 mL of the reconstituted alkaline phosphatase reagent (17 mmol/L p-nitrophenylphosphate and 4 mmol/L magnesium acetate) for 3 h. Normal control human serum (Stanbio Laboratory) of known alkaline phosphatase activity was used as reference. Absorbance at 405 nm was measured directly in the 48-well plate by a microplate reader. Alkaline phosphatase measurements were normalized to the mass of the gel slices to account for differences in the size of the gel slices.

2.12. Alizarin Red S staining

Encapsulated cells were fixed in situ with formalin (Sigma–Aldrich). To stain for calcium deposits, the gel sections were incubated in 1% by mass Alizarin Red S (Sigma–Aldrich) solution (pH 4.3) for 30 min at 22 °C and imaged within the gel on an inverted optical microscope using phase contrast.

2.13. X-ray microcomputed tomography of mineral deposition

Cells within the intact gradient hydrogel samples were fixed in formalin at 42 d and 77 d. For macroscopic examination, gels were photographed with a digital camera (Nikon Coolpix 990). For 3D visualization and quantification of deposited minerals, whole gradients were imaged by X-ray microcomputed tomography (Scanco μ CT 40, 55 kVp, 145 μ A, 15 μ m voxel size (isotropic resolution), 0.3 s integration, 325 slices, sigma 1.2, support 2, threshold 95). A contour region covering the central 90% of the cross-sectional area was selected for analysis. The scanned gradients were analyzed in six segments using instrument software. The threshold value 95 was selected by analyzing voxel intensity histograms from control gradients (freshly-prepared gradient scaffolds without cells or mineral deposits). Threshold of 95 eliminated 99% of the signal from control gradients and was used for all subsequent analysis of gradients with cells and mineral deposits.

2.14. Raman spectroscopy characterization of mineral deposition

Chemical composition of the mineral deposits was examined using a one-laser, broadband coherent anti-Stokes Raman scattering (CARS) system. Control gels of 10% or 20% PEGDM were used for these studies (0.05 mL volume, 5 mm diameter, 2.5 mm thick). Osteoblasts (2.5×10^6 MC3T3-E1 cells/mL) were cultured in the control gels for 21 d, fixed in formalin and cut with a razor into slices approximately 1 mm thick for CARS. CARS was used to image gels with a pixel resolution of 0.5 μ m. Raw CARS spectra were corrected for background using a Kramers–Kronig equivalent transform and averaged over 49 pixels to cover a cell in each image to yield approximate Raman spectra.

2.15. Statistics

All data are presented as mean \pm S.D. (standard deviation) for $n = 3$, unless stated otherwise. Statistical analyses were performed by t -test or 1-way ANOVA with Tukey's test for multiple comparisons (analysis of variance) as indicated in the text. Differences were considered statistically significant for $p < 0.05$.

3. Results

3.1. Fabrication of combinatorial scaffold libraries

PEGDM was prepared by end-functionalizing hydroxyl-terminated PEG following a one-step microwave-assisted reaction [17]. Mass spectrometry indicated that all PEG was functionalized and that it consisted of a mixture of 76% dimethacrylate and 24% monomethacrylate-modified molecules (Fig. 1). When analyzing polymers by mass spectrometry, peak areas are quantitative since polymers are composed of repeating units that ionize in the same manner. There are two sets of peaks in the spectra: i) a larger peak that corresponds in mass to PEGDM (dimethacrylate) and a smaller peak that corresponds to PEGMM (monomethacrylate). The ratio of large to small peak areas is 76:24 for PEGDM:PEGMM.

A combinatorial platform was assembled incorporating a gradient maker to prepare hydrogels with gradients in stiffness (Fig. 2a). In a gradient maker, as liquid of the mixing chamber is drained, it is progressively diluted by contents of the stock chamber creating a gradient in composition of the effluent. For this study, the output of the gradient maker was pumped into a single-entry bottom-filling vertical mold prepared from Teflon sheets and a glass slide [28]. The design of the combinatorial platform affords easy assembly inside a standard hood used to maintain aseptic

conditions for cell culture (Fig. 2b) and is thus well-suited for encapsulating cells within hydrogel scaffolds in situ.

Gradient scaffolds for cell studies were prepared from cells suspended in PEGDM solutions such that the cells were encapsulated within the 3D hydrogel scaffolds. This photopolymerization process has been optimized to minimize cytotoxicity [14]. Although biochemical modification of the polymer network can significantly improve cell survival, no such techniques were applied herein in order to focus on the effect of matrix stiffness. Stiffness was varied by modulating the fraction of PEGDM from 5% to 20% (by mass in solution). Fig. 2c shows a gradient cast in the mold seen through the glass slide wherein trace amounts of a blue dye were added to the 20% solution to make the gradient visible. The cast solution was cured through the glass slide using a 365 nm lamp to obtain gradient gels. For maximal throughput, a mold of 6 cm × 6 cm × 3 mm was designed to cast six gradient samples (6 cm × 1 cm × 3 mm) simultaneously, limited by the minimal and maximal usable volumes for the gradient maker and the dimensions of the lamp window that would ensure uniform curing. Fabrication of gradient hydrogels required approximately 30 min: 15 min to mix the gradient and fill the mold, and another 15 min for photocuring.

3.2. Mechanical characterization of gradient scaffolds

Fig. 3a compiles change in compressive modulus and swelling ratio along the gradient scaffold (statistical analyses in Fig. S1). Modulus increased with increasing fraction of PEGDM and spanned nearly a 30-fold range from ≈ 10 kPa to ≈ 300 kPa. The slope of the modulus change increases from 12 kPa through 74 kPa and then remains constant (linear increase in modulus) through the end of the gradients at 306 kPa. Since the size of a cell (20 μm) is much smaller than the length scale of the changing modulus (centimeters), the changing slope should not affect cell response (each individual cell should sense the same modulus on all of its surfaces). The swelling ratio exhibited a concomitant decrease indicating that softer gels absorbed more water than stiffer gels. Note that Fig. 3a compiles data for 18 samples prepared from three casts. Measurements were repeatable between samples from single and multiple casts.

Moduli and swelling ratios for control gels of uniform composition (Table 1) compared favorably with the measurements on the gradient hydrogels (Fig. 3a) and with previous studies [15]. Though modulus data shown in Fig. 3a and in Table 1 was collected at room temperature (23 °C), the moduli of control 10% and 20% PEGDM gels of uniform composition were measured at 37 °C. Changing temperature from 23 °C to 37 °C did not affect the modulus measurements for 10% or 20% control gels (*t*-test, *n* = 3, *p* > 0.05) indicating that the modulus at room temperature was the same as that experienced by the cells at 37 °C.

Consistent with previous reports [15], the compressive moduli of PEGDM hydrogels soaked in water up to 30 d did not change with

time (*t*-test, *n* = 3, *p* > 0.05). The cross-linked PEGDM network structure was not expected to be susceptible to degradation under the conditions used herein. Note that the mean modulus values at each position in Fig. 3a are used as nominal descriptors to indicate hydrogel gradient position hereafter. The consistency in the modulus and swelling results shows that the combinatorial approach yielded reproducible hydrogel scaffold gradients.

3.3. Measurement of cell response

Three complimentary bioassays were used to measure osteoblast viability/number at each segment of the hydrogel gradients (Fig. 3b; Fig. 4a–c; Fig. S2a–c): 1) Live/Dead stain measures membrane integrity and cellular esterase activity; 2) Wst-1 assay measures cellular metabolic activity (dehydrogenase) and 3) Picrogreen DNA assay measures DNA amount. All three assays detected higher cell numbers at earlier incubation times and in softer regions of the gradients (see Supplementary Information for a more detailed discussion of these data). Cell migration is not a factor in the interpretation of these results since PEG gels are non-degradable which prevents cell migration [29]. These results demonstrate that osteoblast numbers decreased in the hydrogel scaffolds and that cell survival was enhanced in softer segments of the gradients.

Two tests for osteoblastic differentiation were performed, alkaline phosphatase and calcium deposition. Calcium phosphate deposition represents the end result of osteoblast differentiation (mineralization) while alkaline phosphatase represents an earlier marker for osteoblast differentiation. In contrast to cell viability/number, osteoblast differentiation and mineralization increased with increasing culture time and increasing gel modulus, indicated by the enhanced alkaline phosphatase expression (Fig. 3b; Fig. 4d; Fig. S2d) and calcium staining (Fig. 5). For alkaline phosphatase assay (Fig. 4d), results were normalized to the Picrogreen DNA measurements (Fig. 4c) to normalize for cell number (assumes that cell number is proportional to DNA). The same trend of significantly increased alkaline phosphatase expression with increased modulus and culture time was observed when the alkaline phosphatase results were normalized to the Wst-1 results (Fig. S3; also see Supplementary Information for a detailed discussion of the normalization approach). Stains for calcium deposits were first observed at 7 d for 224 kPa and 306 kPa, and were greatly enhanced at 21 d and 42 d (Fig. 5). The 140 kPa regions, but not softer segments, stained positive for calcium at 42 d indicating delayed differentiation with decreased modulus. Longer cultures (>21 d) led to graded mineralization that was visible to the naked eye and scaled with gel stiffness (Fig. 6a).

X-ray microcomputed tomography (μCT) images and volume analysis also demonstrated that mineralization increased with increasing modulus and culture time in the hydrogel gradients (Fig. 6b,c; Fig. S4). Significant mineralization (*p* < 0.05) was observed at modulus 224 kPa and higher for 42 d and 77 d. Although mineralization increased in the 140 kPa segment at 77 d, it was not statistically significant. Using the modulus values of PEGDM gels of known composition (Table 1), it was calculated that gel modulus of 224 kPa corresponds to ≈ 16% PEGDM (by mass). Cross-sectional μCT images of the hydrogels at 42 d show that mineralization occurred in the center of the gels in the lower modulus segments and then increased radially toward the gel edges with increasing modulus (Fig. 6d). It may be that mineral deposition along the edges of the lower modulus gels is hindered since the gel edges are more accessible to medium. This increased accessibility to medium may dilute the secreted minerals and slow their precipitation and deposition at the gel edges relative to the core. Collectively, the mineral staining (Fig. 5), alkaline phosphatase assay (Fig. 4d), and μCT analysis (Fig. 6b–e) demonstrated that

Table 1
Viscosity, Swelling Ratio and Compressive Modulus for Control Gels of Uniform Composition.^a

| PEGDM (by mass) | Viscosity ^b (cP) | Swelling Ratio | Compressive Modulus (kPa) |
|-----------------|-----------------------------|----------------|---------------------------|
| 5% | 1.9 ± 0.0 | 215.4 ± 42.6 | ^c |
| 10% | 3.1 ± 0.1 | 14.7 ± 0.6 | 46 ± 7 |
| 15% | Not measured | 9.7 ± 0.1 | 183 ± 19 |
| 20% | 10.4 ± 0.1 | 7.8 ± 0.1 | 390 ± 14 |

^a All data are means ± S.D., *n* ranged from 4 to 8 for viscosity, *n* was 6 for swelling ratio and *n* was 6 for compressive modulus.

^b Viscosity measurements were performed on aqueous monomer solutions prior to photopolymerization.

^c Modulus was less than the sensitivity of the instrument.

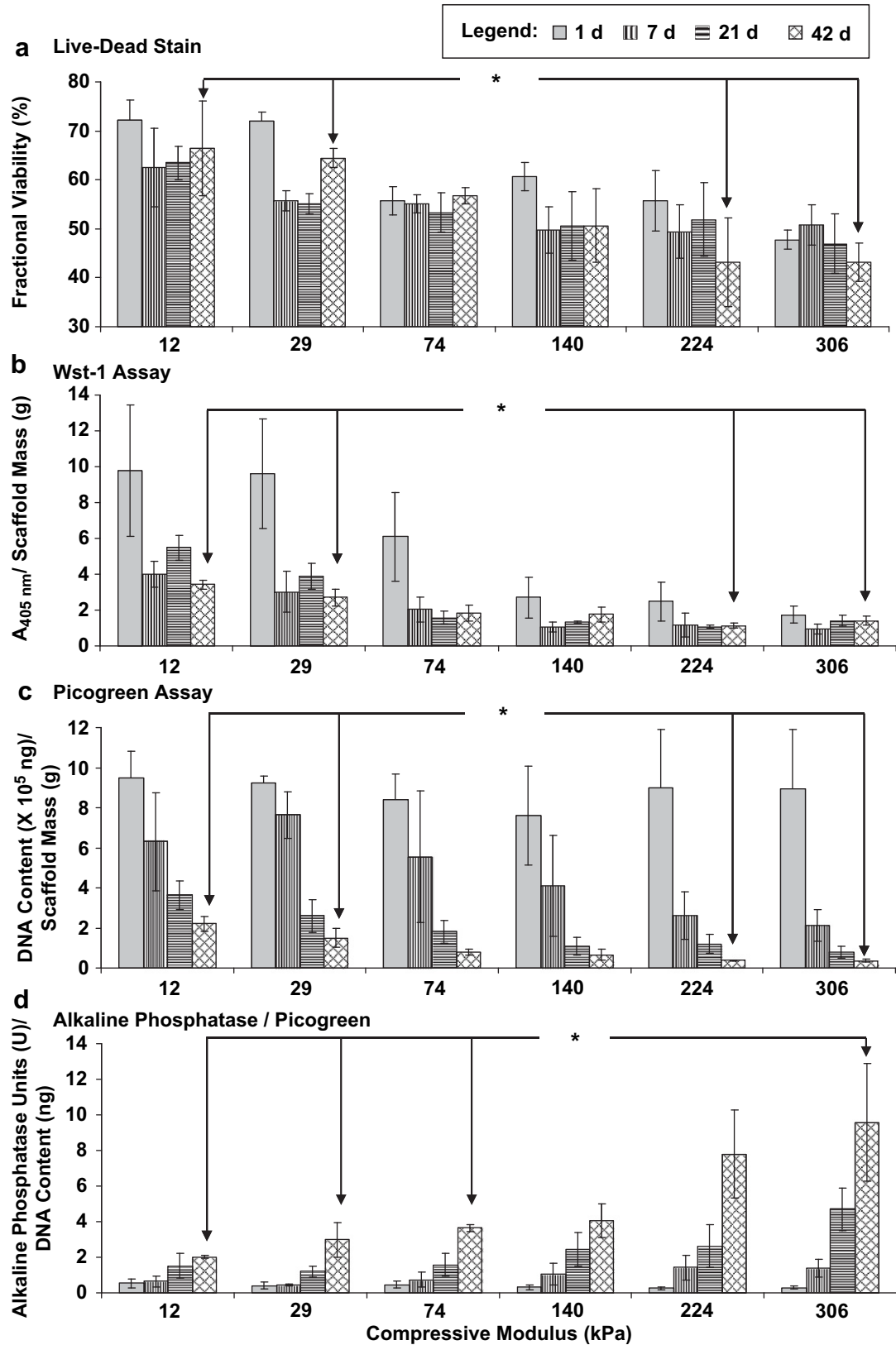


Fig. 4. Cell response in the modulus gradients determined at 1 d (solid gray), 7 d (vertical lines), 21 d (horizontal lines) and 42 d (cross-hatched) for the following tests: (a) fractional viability determined by Live/Dead staining, (b) metabolic activity from Wst-1 assay, (c) DNA content from Picogreen assay, and (d) alkaline phosphatase expression activity normalized to DNA content. Note that all measurements in (b), (c) and (d) were normalized to the mass of the gel slices to account for differences in the size of the gel slice. Error bars are standard deviation and n is 3 for all data points. Statistically significant differences ($p < 0.05$) for 42 d results are indicated by an asterisk (1-way ANOVA with Tukey's) (if an asterisk is encountered when following the line between two data points, then the data points are significantly different). See Fig. S2 for a more complete statistical analysis. The legend provided at the top of the figure applies to all panels (a–d).

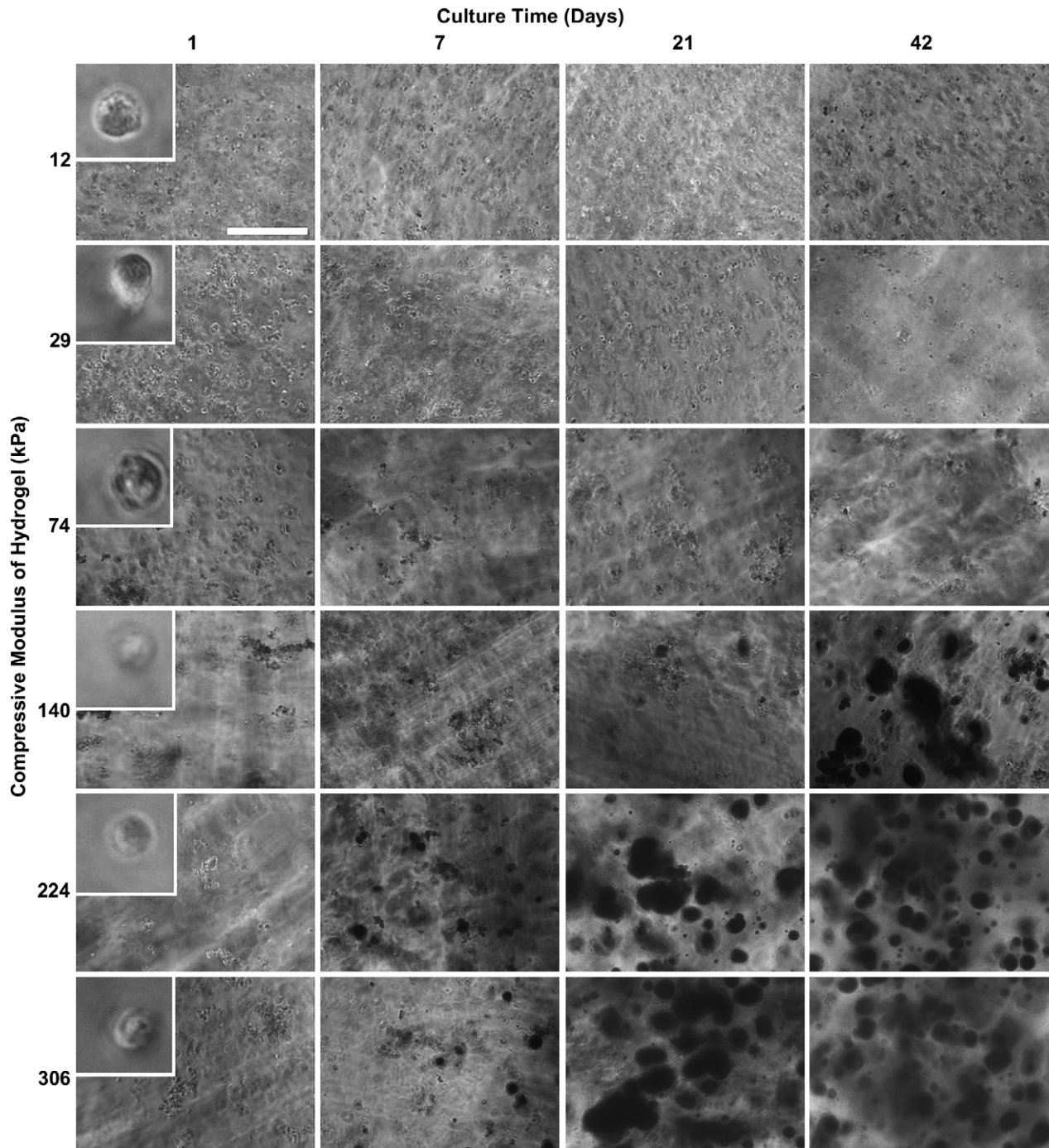


Fig. 5. Representative phase contrast micrographs of gels stained with Alizarin Red S illustrate the spatio-temporal onset and progression of mineral deposition by encapsulated osteoblasts in hydrogel scaffold gradients. Dark patches in the images arise from Alizarin Red S staining of calcium deposits. Scale bar in upper left panel is 0.3 mm and applies to all panels except 1 d insets. The insets in the 1 d panels are 40 μ m across and rounded morphology of encapsulated osteoblasts is seen at all moduli.

increased gel stiffness induced enhanced osteogenic differentiation and subsequent mineralization.

A number of control experiments with uniform composition disc-shaped gels were performed. 10% gels (46 kPa) were selected as a soft gel control and 20% PEGDM gels (390 kPa) were selected as a stiff control (see Table 1 for modulus data of control gels). DNA content for 10% soft control gels with cells was twice as high as for 20% stiff control gels with cells (14 d culture, Picogreen assay, $n = 3$, data not shown), consistent with the gradient experiments that cell numbers were higher in softer gels (Fig. 4a–c). In addition, the stiff

control 20% gels with cells mineralized but soft control 10% gels did not (Fig. 7a) ($n = 3$). These results with control gels validate the results observed for the gradient scaffolds and indicate that the gradient results were not artifacts that arise from the combinatorial platform gradient approach.

In addition, neither 10% nor 20% PEGDM gels without cells cultured in complete cell medium mineralized (Fig. 7a) ($n = 3$). These results confirm that the increased mineralization in stiffer gels was mediated by the osteoblasts. For a positive control, it was observed that addition of osteogenic supplements to the cell

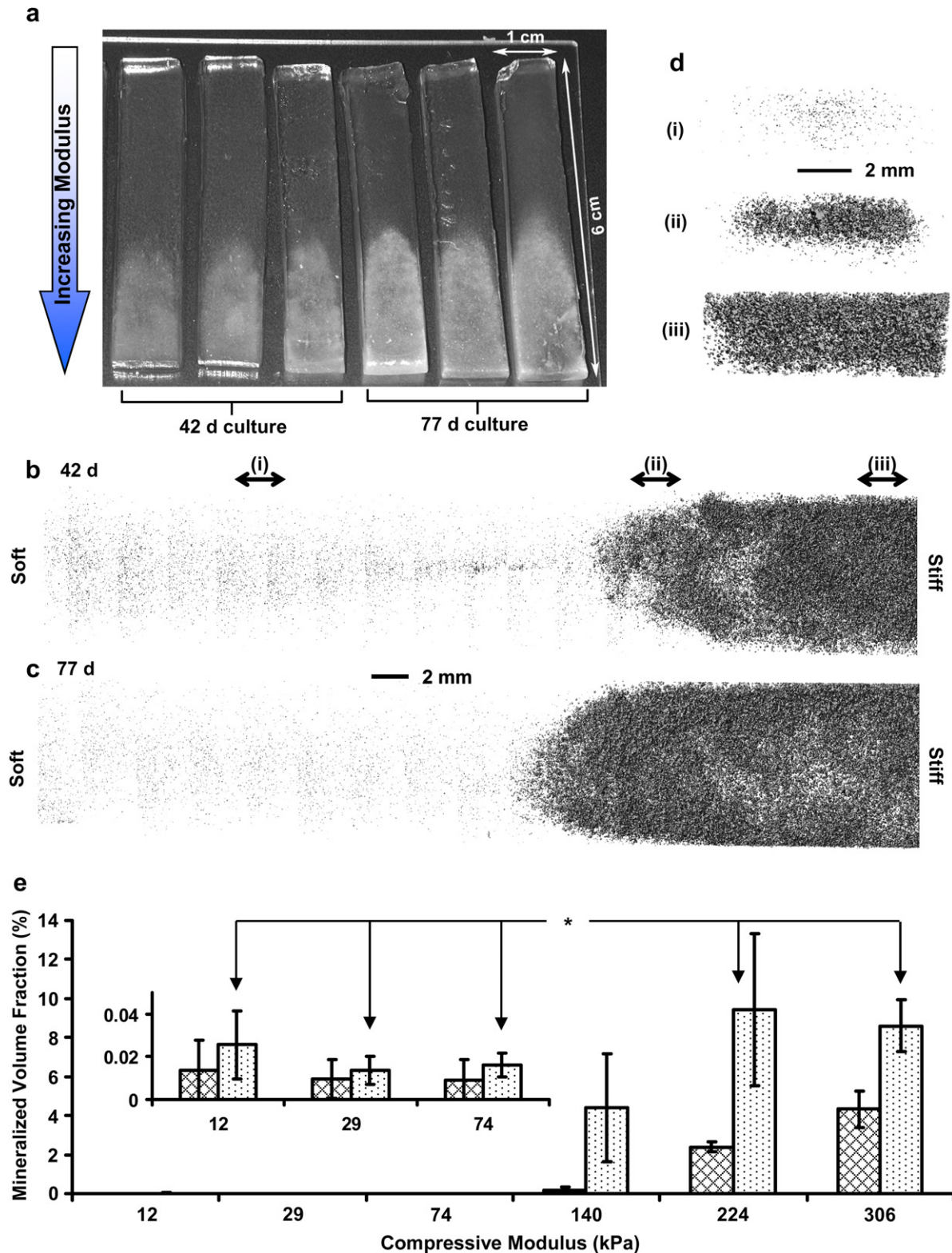


Fig. 6. (a) Photograph of deposited mineral gradients induced by hydrogel stiffness gradients after 42 d and 77 d culture of encapsulated osteoblasts. Deposition of minerals in the stiffer ends of the gradients causes a change in appearance from transparent to white. Representative 3D reconstructions of the mineral deposits in the gradients at 42 d (b) and 77 d (c) from μ CT scans of the hydrogel scaffold gradients. The 3D images shown are composites of scans from the six segments corresponding to the different moduli and the scale bar between (b) and (c) applies to both images. (d) Images present cross-sectional view of the 42 d mineral distribution for 3 mm thick slices at three different positions along the gradient as indicated in (b) by the lower case roman numerals [(i), (ii), (iii)]. Scale bar in (d) applies to all three cross sections. (e) μ CT volume analysis of the mineral content in the gradients at 42 d (cross-hatched) and 77 d (dotted) indicating spatio-temporal differences in mineralization with change in modulus. Inset presents the smaller values for the softer segments. Error bars are standard deviation and n is 3 for all data points. Statistically significant differences ($p < 0.05$) for 77 d results are indicated by an asterisk (1-way ANOVA with Tukey's). If an asterisk is encountered when following the line between two data points, then the data points are significantly different. See Fig. S4 for complete statistical analysis.

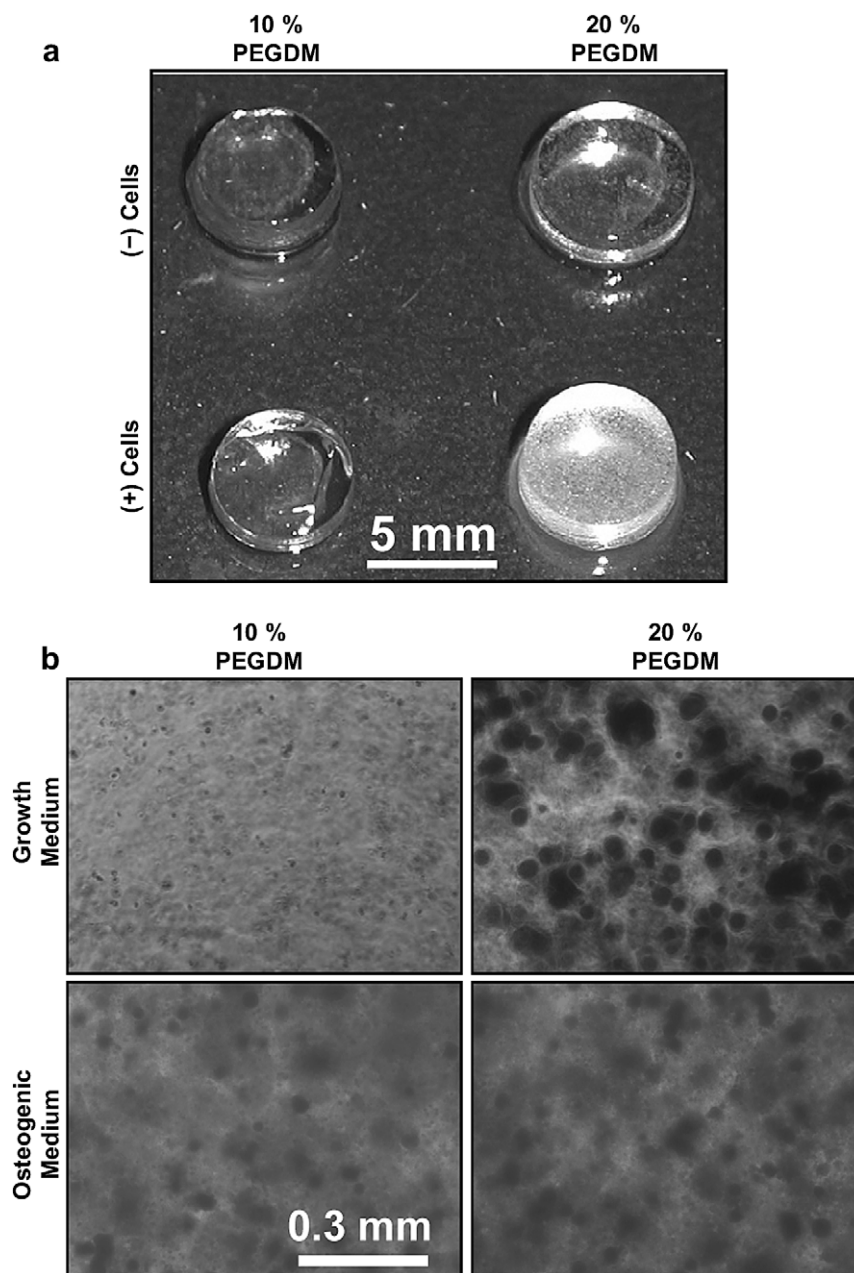


Fig. 7. Control experiments in uniform composition gels validate gradient gel results. (a) Hydrogels of uniform composition were fabricated from 10% or 20% by mass PEGDM with (2.5×10^6 MC3T3-E1 cells/mL) or without cells ($n = 3$). At 56 d, both 10% and 20% PEGDM gels cultured without cells in complete cell medium did not show significant mineralization. The 10% gels (soft) containing cells also did not mineralize while the 20% gels (stiff) containing cells did mineralize. (b) Control experiments to test the effect of osteogenic supplements (dexamethasone, β -glycerophosphate, L-ascorbic acid 2-phosphate) on osteoblast mineralization in PEGDM gels. Hydrogels of uniform composition were fabricated from 10% or 20% by mass PEGDM with MC3T3-E1 cells (2.5×10^6 cells/mL). Cells in gels were cultured for 21 d, fixed, stained for Alizarin Red and imaged.

medium induced osteoblasts to mineralize 10% soft gel controls (Fig. 7b). These results demonstrate that osteoblasts in softer gels are able to respond to osteogenic supplements by mineralizing.

The modulus of mineralized gels was also tested. Control gels of 10% and 20% PEGDM were cultured 21 d with cells and the 10% soft gels did not mineralize while the 20% stiff gels did mineralize (data not shown, similar to samples shown in Fig. 7a). Modulus measurements showed that 21 d culture of the 10% or 20% controls with cells did not have a statistically significant effect on the gel modulus (t -test, $n = 3$, $P > 0.05$, data not shown). These results show that mineralization did not affect gel modulus.

To confirm that mineral deposits were calcium phosphates, Raman spectra were acquired for the gels using coherent anti-Stokes

Raman scattering (CARS) [30]. A vibrational peak at 952 cm^{-1} , characteristic of calcium phosphates present in bony tissue [31], was observed for stiff (20% PEGDM), mineralized gels, but was not present in soft (10% PEGDM), un-mineralized gels (Fig. 8).

4. Discussion

Combinatorial methods are being developed to screen cell–biomaterial interactions to optimize scaffold properties for tissue engineering [3]. Examples include gradients of polymer blends [4], nanoliter arrays of polymer compositions [5], gradients of surface-immobilized biomolecules [6,7], arrays of extracellular matrix proteins [8], and orthogonal gradients to screen

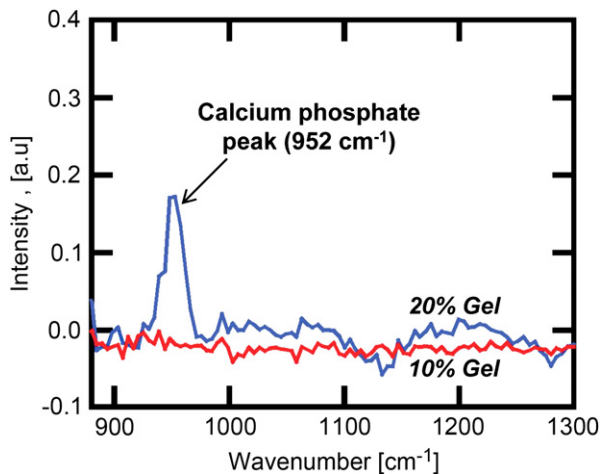


Fig. 8. Coherent anti-Stokes Raman scattering (CARS) imaging was used to analyze the composition of mineral deposits in gels. Osteoblasts encapsulated in control gels of uniform composition (10% PEGDM, red line; 20% PEGDM, blue line) were cultured for 21 d, fixed and imaged by CARS. The softer gels (10% PEGDM, 46 kPa) did not mineralize whereas the stiffer gels (20% PEGDM, 390 kPa) did mineralize, similar to the images shown in Fig. 7a where 20% gels containing cells turned white. The peak at 952 cm^{-1} in the stiffer 20% gels (blue line) corresponds to a vibrational resonance for calcium phosphate, which is not observed in the spectra from the softer 10% gels (red line).

topographical and chemical effects [9,10]. In contrast to the 2D culture format (cells on surfaces) utilized in these methods, a combinatorial technique to fabricate gradients of 3D salt-leached polymer scaffolds for screening cell–scaffold interactions was reported recently [27]. The gradient platform presented in the current work addresses hydrogel scaffolds, enables 3D screening of cell–hydrogel interactions and is both simple and inexpensive to assemble. This platform was applied for identifying optimal hydrogel properties for differentiation of osteoblasts.

A gradient approach afforded systematic screening of cell response to changes in compressive modulus (≈ 10 kPa to ≈ 300 kPa) of hydrogel scaffolds (Fig. 3a). Cell viability/number was measured using a combination of three independent techniques (Live–Dead, Wst-1, Picogreen) and all three indicated a decrease in cell number with increasing modulus and culture time (Fig. 4a–c). Previous work has examined MC3T3-E1 osteoblast response during culture on 2D planar substrates of different compressive moduli. A system of collagen-modified polyacrylamide gels (2D culture) in the presence of osteogenic supplements was used. In contrast to current data, MC3T3-E1 cell number was reported to increase with increasing compressive modulus (measured at 11 kPa, 21 kPa and 39 kPa) [32]. However, the current results in 3D (Fig. 4d; Fig. 5; Fig. 6a–d) concur with the previous 2D observations that MC3T3-E1 differentiation and mineralization increase with increasing modulus [32].

There is growing consensus that physical properties of materials, such as topography, geometry, porosity and stiffness, can be used to direct biological outcomes in a manner similar to traditional approaches involving chemistry or biomolecules [33–36]. Previous studies with planar substrates (2D culture) have shown that stiffness of the underlying surface affects cellular behaviors such as proliferation, organization, migration and differentiation [33,35,36]. For previous work with osteoblasts in particular, proliferation of rat calvarial cells was enhanced on stiffer poly(*N*-isopropylacrylamide-co-acrylic acid) gels (2D) compared to softer gels [37]. Organization, motility and supplement-induced differentiation of MC3T3-E1 osteoblasts cultured on collagen-modified polyacrylamide gels and arginine-glycine-aspartate (RGD)-modified PEG hydrogels (2D)

were influenced by matrix stiffness [38,39]. In a few studies, cell response to matrix stiffness has also been investigated in 3D culture [15,16,40]. Chondrocytes seeded within PEG hydrogels in chondrogenic media deposited a maximum amount of glycosaminoglycans at an optimal modulus [15]. Gel stiffness influenced differentiation of encapsulated cardioprogenitor cells in degradable PEG hydrogels [40]. Interestingly, it has been observed that phenotypic response of smooth muscle cells to changes in matrix modulus varied markedly in 3D culture (in gels) from that observed on 2D substrates (on gels) [16]. The current work demonstrates that scaffold mechanical properties influence osteoblast differentiation and mineralization in 3D.

It is widely believed that cells sense the stiffness of their environment and when cultured *in vitro* they behave most physiologically when the stiffness of the underlying substrate (2D format) matches the tissue modulus *in vivo* [35,36]. Soft (non-mineralized) collagenous bone is believed to have a stiffness of ≈ 100 kPa [35]. Interestingly, for the mineralized gradients generated in this study, essentially no mineral deposits were observed for scaffold segments softer than 100 kPa (Figs. 5 and 6e). For stiffer segments with moduli > 100 kPa, the volume of minerals deposited increased with increasing modulus, although the volume in the 140 kPa segment was not statistically significant. Therefore, these results indicate that differentiation of osteoblasts in the 3D hydrogel scaffolds was maximized when the modulus of the scaffold matched the modulus of mineralized bone tissue *in vivo*. The intracellular signaling pathways that direct cell response to scaffold stiffness are poorly understood and are an active area of research. Recent work with MC3T3-E1 cells in 2D culture indicates that the extracellular signal-regulated kinase/mitogen-activated protein kinase (ERK/MAPK) signaling pathway could be playing an important role [38].

In this study, 3D hydrogel modulus was varied by changing percent PEGDM composition whereby higher PEGDM composition yielded higher modulus gels. Increased gel modulus is associated with increased cross-link density and a reduction in correlation length (distance between polymer-rich domains or cross-linking points), with the latter affecting diffusion of molecules within the gel. However, previous studies using small angle neutron scattering found that the correlation lengths for cross-linked PEGDM gels were similar for 10%, 20% and 30% gels (11 nm, 11 nm and 9 nm, respectively) indicating that diffusion rates would be similar [41]. In addition, the diffusion constant of Toluidine blue (MW 306 g/mol) was observed to be nearly the same for 5% and 10% poly(ethylene glycol) diacrylate (PEGDA) gels (PEG MW = 6000 g/mol; $D_{5\%} = 1.2 \times 10^{-5}\text{ cm}^2/\text{s}$; $D_{10\%} = 0.99 \times 10^{-5}\text{ cm}^2/\text{s}$), which are very similar to the PEGDM gel system used herein [42]. These results suggest that diffusion rates should be similar in the different regions of the PEGDM gradient gels fabricated in this study.

It is also unlikely that chemistry varies significantly within the gradient gels. For the PEGDM molecules used in this study, there are only 2 methacrylate groups for every 91 repeat units of ethylene glycol. PEGDM in the pre-polymer solutions contains greater than 96% PEG (by mass) and only 4% methacrylate. Fewer free methacrylate groups will be available after photopolymerization such that there will be essentially no difference in chemistry along the gradient.

Although the cell morphology was predominantly spherical at all moduli in the gradients (Fig. 5 insets), there was an increase in clustering of encapsulated cells with increasing gel stiffness (Fig. 5). The clustering was not caused by the gradient fabrication process because it was also observed in stiff gels of uniform composition (like those shown in Fig. 7). Clumping was observed immediately after photopolymerization of stiff gels suggesting that the polymerization process caused the clumping. The rapid cross-link

reaction in the more concentrated solutions likely excludes cells leading to areas where cells are closer together.

Ligaments transition from soft, non-mineralized connective tissue into harder, mineralized bone tissue spanning a compressive modulus range of ≈ 100 kPa to ≈ 1000 kPa [18], comparable to the range afforded by the graded scaffolds herein (≈ 10 kPa to ≈ 300 kPa). Studies to generate continuous interfaces with engineered bone have been reported previously [43–45]. Triphasic scaffolds have been fabricated from two polymers and a bioglass and used to co-culture fibroblasts and osteoblasts towards engineering the bone–ligament interface [43]. More recently, graded retroviral delivery of an osteoblast transcription factor (Runx2) from a collagen scaffold to seeded fibroblasts was used to generate a gradient construct for ligament engineering [44]. Others have fabricated graded osteochondral constructs by culturing mesenchymal stem cells seeded on scaffolds containing opposing gradients in growth factors: bone morphogenic protein (BMP-2) for inducing osteogenesis and insulin-like growth factor (IGF-1) for inducing chondrogenesis [45].

The gradients constructed herein were designed for combinatorial screening and were 6 cm in length. The point of insertion for anterior cruciate ligament has a gradient from ligament to fibrocartilage to bone that spans several mm [43]. Thus, the length scale of the current gradient system could be reduced from cm to mm in order to match the length scale of the gradients found in ligament *in vivo*.

Results presented in this study indicate that gradients in scaffold stiffness (compressive modulus) can be leveraged towards engineering seamless tissue interfaces between bone and soft tissues. The current approach for fabricating a mineralized tissue gradient is unique because only a single material (PEGDM) was used and only a physical property (modulus) of the scaffold was varied. Graded osteogenesis was induced without the use of expensive, labile or potentially carcinogenic bioactive factors (proteins, peptides, growth factors, vectors) [22]. Moreover, the graded tissue generated herein did not require the addition of osteogenic supplements to the medium and was fabricated with osteoblasts *in situ*. It may, therefore, be possible to augment tissue regeneration *in situ* by modulation of the mechanical properties of these injectable hydrogels without use of bioactive factors.

5. Conclusion

This work presents a combinatorial method for screening cell–material interactions in a 3D cell culture format that mimics the 3D environment of cells *in vivo*. This platform was utilized to fabricate gradient hydrogel scaffolds with osteoblasts encapsulated *in situ* containing a 30-fold range in compressive modulus within a single specimen (≈ 10 kPa to ≈ 300 kPa). Results presented herein demonstrate that mechanical properties of the matrix influence differentiation of osteoblasts in 3D in the absence of biochemical cues in the form of supplements, immobilized biomolecules or vectors. The gradients enabled systematic screening of osteoblast differentiation and demonstrated that hydrogels of modulus ≈ 225 kPa ($\approx 16\%$ PEGDM by mass) or higher were required for inducing significant mineralization. In addition, these results demonstrate that variation of only a material property, compressive modulus, can be used to induce graded osteogenesis and generation of a mineralized tissue gradient that could be applied to integrate hard and soft tissues such as a tendon or a ligament.

Acknowledgements

Authors gratefully acknowledge technical assistance from Kathy Flynn (NIST) and Ed Parry (ADA-NIST) and insightful discussions

with Kathryn L. Beers (NIST). This research was performed while K.C. and S.H.P. held Research Associateship Awards from the National Research Council of the National Academy of Sciences in the Joint NIH-NIBIB/NIST and the NIST Postdoctoral Programs, respectively (National Institutes of Health-National Institute of Biomedical Imaging and Bioengineering/National Institute of Standards and Technology). This work was supported by NIST, NIH/NIBIB R21 EB006497-01 and the Intramural Program of the NIH/NIDCR (National Institute of Dental and Craniofacial Research). The “standard deviation” (S.D.) is the same as the “combined standard uncertainty of the mean” for the purposes of this work. The content is solely the responsibility of the authors and does not necessarily represent the official views of NIH, NIBIB, NIDCR or NIST. This article, a contribution of NIST, is not subject to US copyright. Certain equipment and instruments or materials are identified in the paper to adequately specify the experimental details. Such identification does not imply recommendation by NIST, nor does it imply the materials are necessarily the best available for the purpose.

Appendix. Supplementary data

Supplementary data associated with this article can be found in the on-line version, at doi:10.1016/j.biomaterials.2010.03.024.

Appendix

Figures with essential colour discrimination. Most of the figures in this article may be difficult to interpret in black and white. The full colour images can be found in the on-line version, at doi:10.1016/j.biomaterials.2010.03.024.

References

- [1] Place ES, Evans ND, Stevens MM. Complexity in biomaterials for tissue engineering. *Nat Mater* 2009;8(6):457–70.
- [2] Lysaght MJ, Jaklencic A, Deweerd E. Great expectations: private sector activity in tissue engineering, regenerative medicine, and stem cell therapeutics. *Tissue Eng A* 2008;14(2):305–15.
- [3] Simon CG, Yang Y, Thomas V, Dorsey SM, Morgan AW. Cell interactions with biomaterials gradients and arrays. *Comb Chem High Throughput Screen* 2009;12(6):544–53.
- [4] Meredith JC, Sormana JL, Keselowsky BG, Garcia AJ, Tona A, Karim A, et al. Combinatorial characterization of cell interactions with polymer surfaces. *J Biomed Mater Res A* 2003;66(3):483–90.
- [5] Anderson DG, Levenberg S, Langer R. Nanoliter-scale synthesis of arrayed biomaterials and application to human embryonic stem cells. *Nat Biotechnol* 2004;22(7):863–6.
- [6] Gallant ND, Lavery KA, Amis EJ, Becker ML. Universal gradient substrates for “click” biofunctionalization. *Adv Mater* 2007;19:965–9.
- [7] DeLong SA, Gobin AS, West JL. Covalent immobilization of RGDS on hydrogel surfaces to direct cell alignment and migration. *J Control Release* 2005;109(1–3):139–48.
- [8] Flaim CJ, Chien S, Bhatia SN. An extracellular matrix microarray for probing cellular differentiation. *Nat Methods* 2005;2(2):119–25.
- [9] Yang J, Rose FRAJ, Gadegaard N, Alexander MR. A high-throughput assay of cell–surface interactions using topographical and chemical gradients. *Adv Mater* 2009;21(3):300–4.
- [10] Lovmand J, Justesen J, Foss M, Lauridsen RH, Lovmand M, Modin C, et al. The use of combinatorial topographical libraries for the screening of enhanced osteogenic expression and mineralization. *Biomaterials* 2009;30(11):2015–22.
- [11] Fischbach C, Chen R, Matsumoto T, Schmelzle T, Brugge JS, Polverini PJ, et al. Engineering tumors with 3D scaffolds. *Nat Methods* 2007;4(10):855–60.
- [12] Cushing MC, Anseth KS. Material science: hydrogel cell cultures. *Science* 2007;316(5828):1133–4.
- [13] Elisseeff J, Anseth KS, Sims D, McIntosh W, Randolph M, Yaremchuk M, et al. Transdermal photopolymerization of poly (ethylene oxide)-based injectable hydrogels for tissue-engineered cartilage. *Plast Reconstr Surg* 1999;104(4):1014–22.
- [14] Williams CG, Malik AN, Kim TK, Manson PN, Elisseeff JH. Variable cytocompatibility of six cell lines with photoinitiators used for polymerizing hydrogels and cell encapsulation. *Biomaterials* 2005;26(11):1211–8.
- [15] Bryant SJ, Anseth KS. Hydrogel properties influence ECM production by chondrocytes photoencapsulated in poly(ethylene glycol) hydrogels. *J Biomed Mater Res* 2002;59(1):63–72.

- [16] Peyton SR, Kim PD, Ghajar CM, Seliktar D, Putnam AJ. The effects of matrix stiffness and RhoA on the phenotypic plasticity of smooth muscle cells in a 3-D biosynthetic hydrogel system. *Biomaterials* 2008;29(17):2597–607.
- [17] Lin-Gibson S, Bencherif S, Cooper JA, Wetzel SJ, Antonucci JM, Vogel BM, et al. Synthesis and characterization of PEG dimethacrylates and their hydrogels. *Biomacromolecules* 2004;5(4):1280–7.
- [18] Moffat KL, Sun W-HS, Pena PE, Chahine NO, Doty SB, Ateshian GA, et al. Characterization of the structure-function relationship at the ligament-to-bone interface. *Proc Natl Acad Sci U S A* 2008;105(23):7947–52.
- [19] Kishen A, Ramamurthy U, Asundi A. Experimental studies on the nature of property gradients in the human dentine. *J Biomed Mater Res* 2000;51(4):650–9.
- [20] Beaulieu JF. Integrins and human intestinal cell functions. *Front Biosci* 1999;4:310–21.
- [21] Lander AD. Morphus unbound: reimagining the morphogen gradient. *Cell* 2007;128(2):245–56.
- [22] Katsuno Y, Hanyu A, Kanda H, Ishikawa Y, Akiyama F, Iwase T, et al. Bone morphogenetic protein signaling enhances invasion and bone metastasis of breast cancer cells through Smad pathway. *Oncogene* 2008;27(49):6322–33.
- [23] Sudo H, Kodama H, Amagai Y, Yamamoto S, Kasai S. In vitro differentiation and calcification in a new clonal osteogenic cell line derived from newborn mouse calvaria. *J Cell Biol* 1983;96(1):191–8.
- [24] Powell K, Leslie M. Dishing up bone formation. *J Cell Biol* 2005;171:409.
- [25] Stein GS, Lian JB, Owen TA. Relationship of cell-growth to the regulation of tissue-specific gene-expression during osteoblast differentiation. *FASEB J* 1990;4(13):3111–23.
- [26] Choi JY, Lee BH, Song KB, Park RW, Kim IS, Sohn KY, et al. Expression patterns of bone-related proteins during osteoblastic differentiation in MC3T3-E1 cells. *J Cell Biochem* 1996;61(4):609–18.
- [27] Yang Y, Bolikal D, Becker ML, Kohn J, Zeiger D, Simon Jr CG. Combinatorial polymer scaffold libraries for screening cell-biomaterial interactions in 3D. *Adv Mater* 2008;20(11):2037–43.
- [28] Xu C, Barnes SE, Wu T, Fischer DA, DeLongchamp DM, Batteas JD, et al. Solution and surface composition gradients via microfluidic confinement: fabrication of a statistical-copolymer-brush composition gradient. *Adv Mater* 2006;18:1427–30.
- [29] Kloxin AM, Kasko AM, Salinas CN, Anseth KS. Photodegradable hydrogels for dynamic tuning of physical and chemical properties. *Science* 2009;324(5923):59–63.
- [30] Lee YJ, Cicerone MT. Single-shot interferometric approach to background free broadband coherent anti-stokes Raman scattering spectroscopy. *Opt Express* 2009;17(1):123–35.
- [31] Sauer GR, Zunic WB, Durig JR, Wuthier RE. Fourier-transform Raman-spectroscopy of synthetic and biological calcium phosphates. *Calcif Tissue Int* 1994;54(5):414–20.
- [32] Khatiwala CB, Peyton SR, Putnam AJ. Intrinsic mechanical properties of the extracellular matrix affect the behavior of pre-osteoblastic MC3T3-E1 cells. *Am J Physiol-Cell Physiol* 2006;290(6):C1640–50.
- [33] Mitragotri S, Lahann J. Physical approaches to biomaterial design. *Nat Mater* 2009;8(1):15–23.
- [34] Dalby MJ, Gadegaard N, Tare R, Andar A, Riehle MO, Herzyk P, et al. The control of human mesenchymal cell differentiation using nanoscale symmetry and disorder. *Nat Mater* 2007;6(12):997–1003.
- [35] Engler AJ, Sen S, Sweeney HL, Discher DE. Matrix elasticity directs stem cell lineage specification. *Cell* 2006;126(4):677–89.
- [36] Saha K, Keung AJ, Irwin EF, Li Y, Little L, Schaffer DV, et al. Substrate modulus directs neural stem cell behavior. *Biophys J* 2008;95(9):4426–38.
- [37] Chung EH, Gilbert M, Virdi AS, Sena K, Sumner DR, Healy KE. Biomimetic artificial ECMs stimulate bone regeneration. *J Biomed Mater Res A* 2006;79A(4):815–26.
- [38] Khatiwala CB, Kim PD, Peyton SR, Putnam AJ. ECM compliance regulates osteogenesis by influencing MAPK signaling downstream of RhoA and ROCK. *J Bone Miner Res* 2009;24(5):886–98.
- [39] Hsiong SX, Carampin P, Kong H-J, Lee K-Y, Mooney DJ. Differentiation stage alters matrix control of stem cells. *J Biomed Mater Res A* 2008;85A(1):145–56.
- [40] Kraehenbuehl TP, Zammaretti P, Van der Vlies AJ, Schoenmakers RG, Lutolf MP, Jaconi ME, et al. Three-dimensional extracellular matrix-directed cardioprogenitor differentiation: systematic modulation of a synthetic cell-responsive PEG-hydrogel. *Biomaterials* 2008;29(18):2757–66.
- [41] Lin-Gibson S, Jones RL, Washburn NR, Horkay F. Structure-property relationships of photopolymerizable poly(ethylene glycol) dimethacrylate hydrogels. *Macromolecules* 2005;38(7):2897–902.
- [42] Cuchiara MP, Miller JS, West JL. Perfusible cell laden microchannel networks in poly(ethylene glycol) hydrogels. *Transactions of the 33rd Annual Meeting of the Society for Biomaterials* 2010;31:254.
- [43] Spalazzi JP, Doty SB, Moffat KL, Levine WN, Lu HH. Development of controlled matrix heterogeneity on a triphasic scaffold for orthopedic interface tissue engineering. *Tissue Eng* 2006;12(12):3497–508.
- [44] Phillips JE, Burns KL, Le Doux JM, Guldborg RE, Garcia AJ. Engineering graded tissue interfaces. *Proc Natl Acad Sci U S A* 2008;105(34):12170–5.
- [45] Wang X, Wenk E, Zhang X, Meinel L, Vunjak-Novakovic G, Kaplan DL. Growth factor gradients via microsphere delivery in biopolymer scaffolds for osteochondral tissue engineering. *J Control Release* 2009;134(2):81–90.

Supplementary Information

The Effect of 3D Hydrogel Scaffold Modulus on Osteoblast Differentiation and Mineralization Revealed by Combinatorial Screening

Kaushik Chatterjee, Sheng Lin-Gibson, William E. Wallace, Sapun H. Parekh, Young Jong Lee, Marcus T. Cicerone, Marian F. Young, Carl G. Simon, Jr.

Discussion of Live/Dead, Wst-1, Picogreen and Alkaline Phosphatase Assays:

Introduction: Three standard assays for measuring cell viability/number (Live/Dead, Wst-1 and Picogreen) were used. Since each has its own strengths and weaknesses, all three were performed for a more robust analysis.

Live-Dead staining is a semi-quantitative or qualitative measure of cell viability and number. The Dead stain labels nucleic acids of cells with leaky membranes (membranes rapidly breakdown when cells die). The Live stain accumulates in cells with intact membranes that have active esterase enzymes (both requisite of live cells). Note that esterase activity may vary with cell proliferation/differentiation state in addition to viability state. Also note that intact gels are required for this assay which means that diffusion of the Live-Dead stains into the gels may not be uniform. The advantage of the Live-Dead assay compared to Wst-1 and Picogreen is that Live-Dead yields images which are invaluable for general assessment of cell distribution, morphology and viability in the gels (neither Wst-1 nor Picogreen assays yield images). Live-Dead is also a more immediate indicator for loss of viability than Picogreen since esterase activity is lost before DNA degrades.

Wst-1 assays measures cellular metabolic activity (dehydrogenase) which may vary with cell proliferation/differentiation state in addition to viability state. In addition, gels and cells must be intact for this assay (all activity was lost if specimens were dounce-homogenized). Thus, diffusion of the Wst-1 reactant into the gels may not be uniform. However, Wst-1 is quantitative. Wst-1 is also a more immediate indicator for loss of viability than Picogreen since dehydrogenase activity is lost before DNA degrades.

Picogreen assay measures the amount of DNA. Note that amount of DNA may vary with cell proliferation/differentiation state in addition to with viability state. Also note that gels were homogenized for this assay to enable DNA extraction (this is the only assay of the three cell number/viability tests where gels were homogenized). Thus, non-uniform diffusion of stains or reactants into gels is not a concern. In addition, Picogreen is quantitative. However, dead cells may contribute to the Picogreen signal since it can take time for DNA to degrade.

Comparison of Live/Dead, Wst-1 and Picogreen: There is a consistent trend of decreasing cell viability/number with increasing culture time and increasing gel modulus as measured by Live-Dead, Wst-1 and Picogreen (Fig. 4). However, some subtle differences exist between the data from the three assays. For instance, the 1 d data for Picogreen shows no change in cell number with increasing modulus while Live-Dead and Wst-1 show a decrease in cell viability/number with increasing modulus for 1 d. Since DNA can take longer than 1 d to degrade, the Picogreen assay detects the presence of the dead cells after 1 d. However, esterase and dehydrogenase activity of dead cells will rapidly drop causing the Live-Dead and Wst-1 assays to detect a decrease in cell viability/number after 1 d in the high modulus gels. In sum, the three bioassays of Live-Dead, Wst-1 and Picogreen provide complimentary data that prove a more complete view of cell viability/number in the hydrogel gradients. There is a clear opportunity for the development of improved methods for quantifying cell viability/number in hydrogels.

Normalization of Alkaline Phosphatase Data: Gene expression results such as alkaline phosphatase assays are typically normalized to cell number data to yield “expression level per cell” (Franceschi et al., 1992; Choi et al., 1996; Lee et al., 2006). This makes it possible to determine i) if increased expression levels are a result of cell proliferation where “expression per cell” does not change or ii) if individual cells are expressing higher overall levels of the gene. Herein, alkaline phosphatase results were normalized to DNA in Fig. 4d. Alkaline phosphatase was normalized to DNA because the Picogreen assay has a calibration standard curve. The standard curve makes it possible to compare more directly data from assays run on different days. The alkaline phosphatase data can also be normalized to the Wst-1 metabolic assay as shown in Fig. S3. The Wst-1 metabolic assay does not have a standard calibration curve which makes comparisons of Wst-1 assay data run on different days less comparable. For these reasons, alkaline phosphatase was normalized to DNA in the main figures and was normalized to Wst-1 metabolic data in the Supplementary Information (Fig. S3). The conclusions from the alkaline phosphatase tests are the same whether the data are normalized to DNA or Wst-1, that alkaline phosphatase expression level per cell is enhanced with increasing modulus in 3D PEGDM gels (Fig. 4d, Fig. S2d, Fig. S3).

Supplementary References

- Franceschi RT, Iyer BS. Relationship Between Collagen Synthesis and Expression of the Osteoblast Phenotype in MC3T3-E1 Cells. *J Bone Miner Res* 1992;2(2):235-46.
- Choi J-Y, Lee B-H, Song K-B, Park R-W, Kim I-S, Sohn K-Y, Jo J-S, Ryoo H-M. Expression Patterns of Bone-Related Proteins During Osteoblastic Differentiation in MC3T3-E1 Cells. *J Cell Biochem* 1996;61(4):609-18.
- Lee DH, Park BJ, Min-sub Lee, Lee JW, Kim JK, Yang H-C, Park J-C. Chemotactic Migration of Human Mesenchymal Stem Cells and MC3T3-E1 Osteoblast-Like Cells Induced by COS-7 Cell Line Expressing rhBMP-7. *Tiss Eng* 2006;12(6)1577-86.

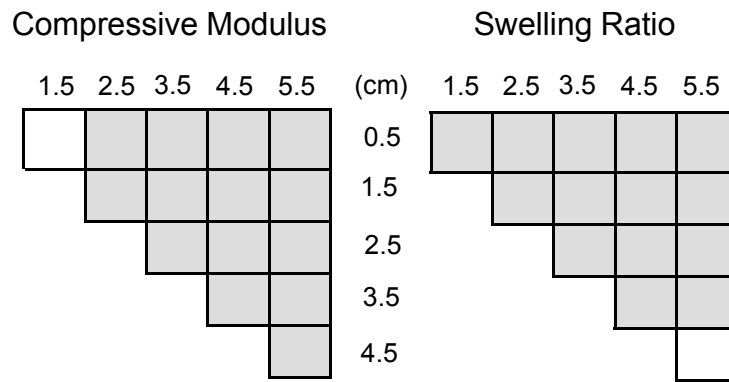
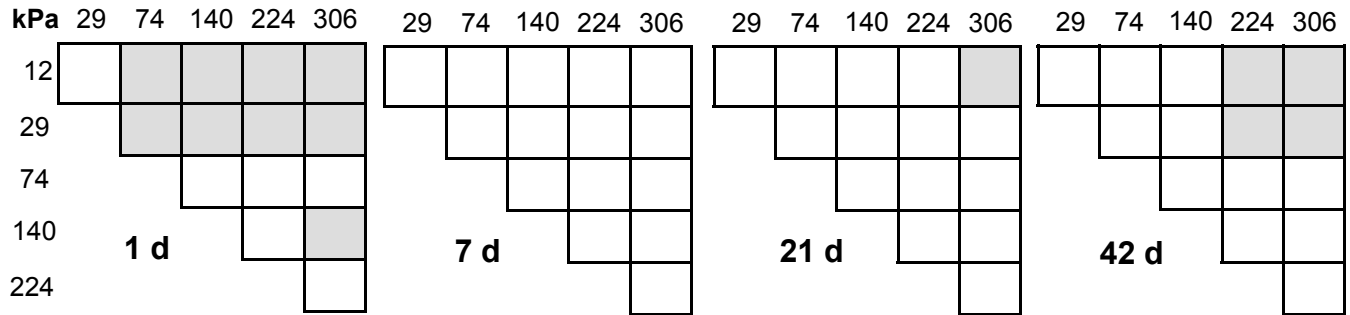
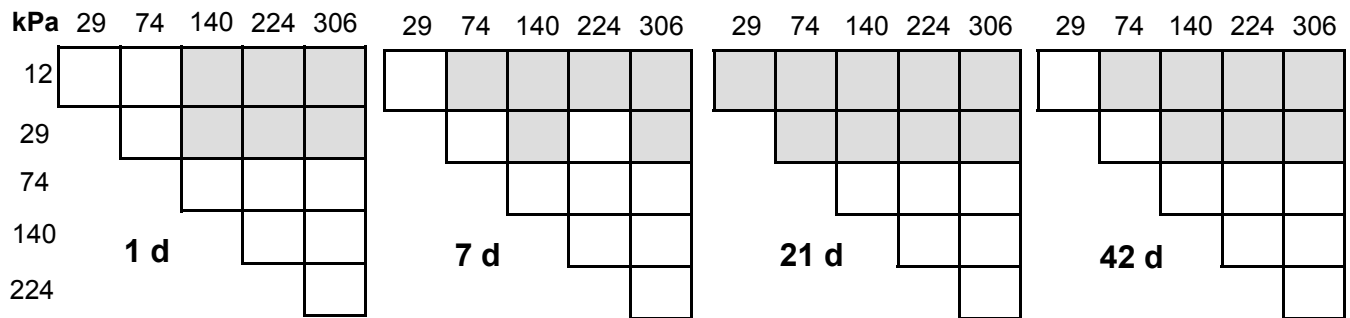


Figure S1. Statistical analysis of compressive modulus and swelling ratio of the hydrogels along the gradients presented in Fig. 3a. The numbers in the margins of the figure indicate position in the gradient scaffolds. Grey squares indicate that differences are statistically significant ($p < 0.05$, 1-way ANOVA with Tukey's), whereas white squares indicate no statistical significance ($p > 0.05$).

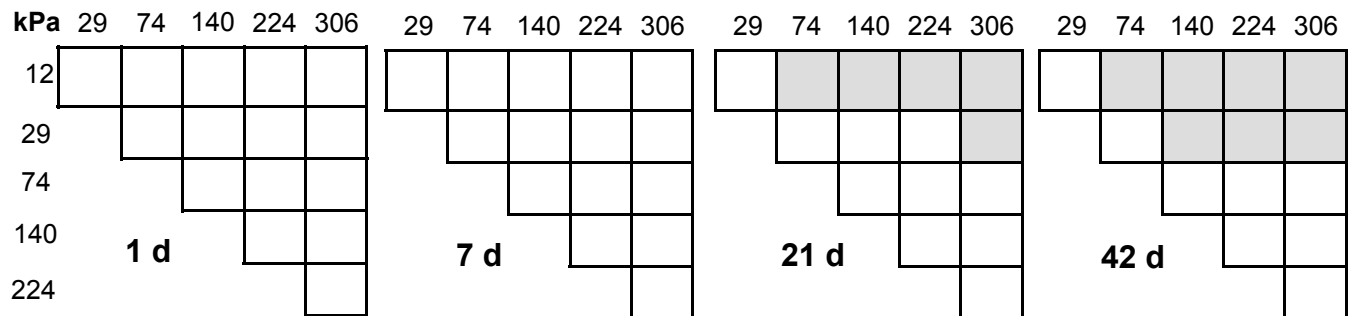
(a) Fractional Viability: Live/Dead Stain



(b) Metabolic Activity: Wst-1 Assay



(c) DNA Content: Picogreen Assay



(d) Alkaline Phosphatase Expression: Alk. Phos. Assay/Picogreen

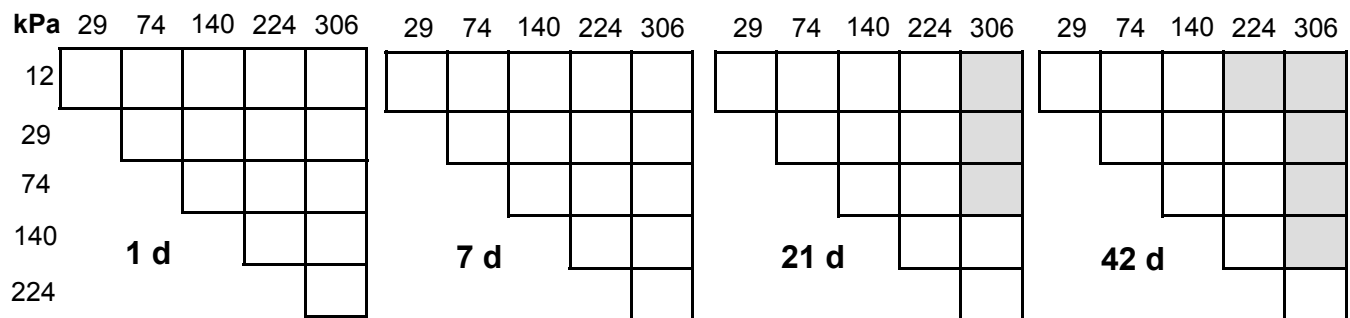
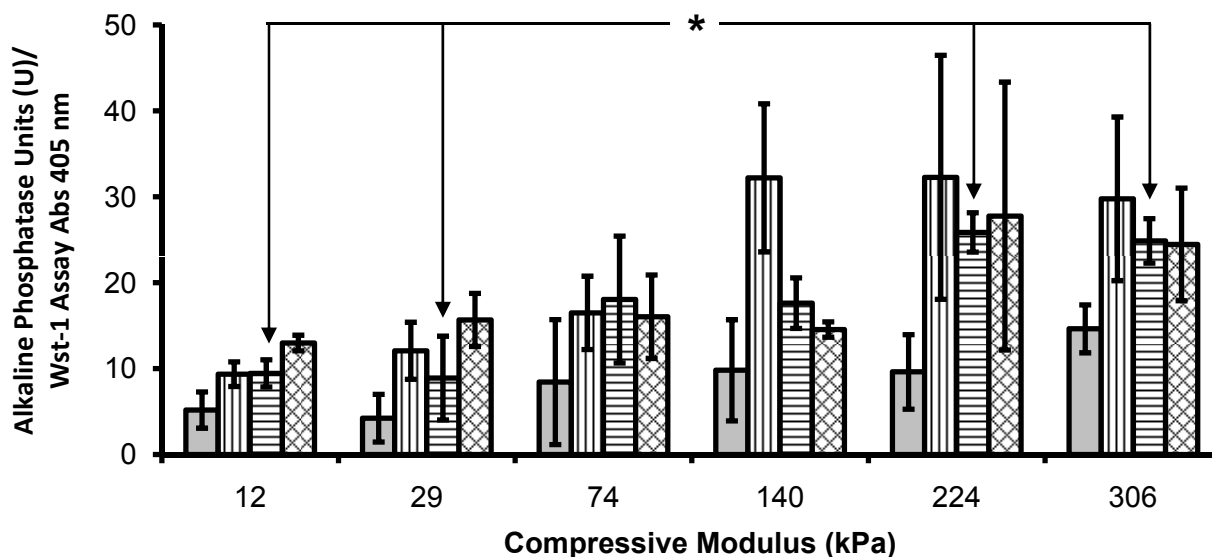


Figure S2. Statistical analyses (1-way ANOVA with Tukey's) of (a) fractional viability, (b) metabolic activity, (c) DNA content, and (d) alkaline phosphatase expression measurements presented in Fig. 4. Numbers in the margins indicate modulus from the gradient scaffolds. Grey squares indicate statistically significant differences ($p < 0.05$), whereas white squares indicate no statistical significance ($p > 0.05$).

(a) Alkaline Phosphatase / Wst-1



(b) Statistics: Alkaline Phosphatase / Wst-1

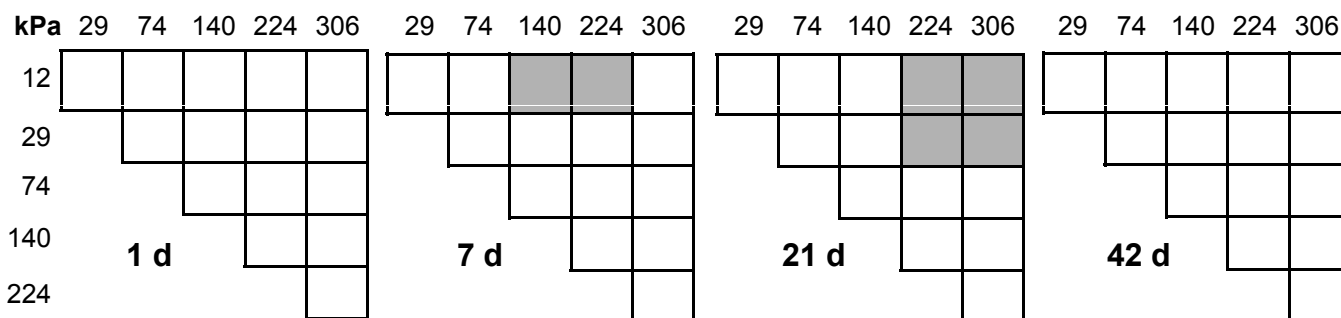


Figure S3. Alkaline phosphatase activity normalized to Wst-1 activity. (a) Alkaline phosphatase activity normalized to Wst-1 activity in the modulus gradients determined at 1 d (solid gray), 7 d (vertical lines), 21 d (horizontal lines) and 42 d (cross-hatched). All measurements were normalized to the mass of the gel slices to account for differences in the size of the gel slice. Error bars are standard deviation and n is 3 for all data points. Statistically significant differences ($p < 0.05$) for 21 d results are indicated by an asterisk (ANOVA with Tukey's) (if an asterisk is encountered when following the line between two data points, then the data points are significantly different). (b) Complete statistical analyses (1-way ANOVA with Tukey's) of alkaline phosphatase data normalized to Wst-1 activity shown in Panel (a). Numbers in the margins indicate modulus from the gradient scaffolds. Grey squares indicate statistically significant differences ($p < 0.05$), whereas white squares indicate no statistical significance ($p > 0.05$).

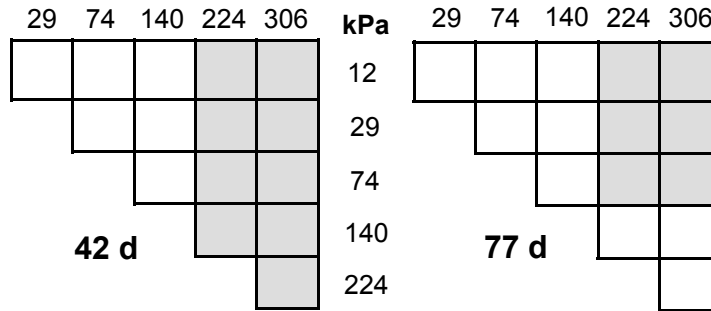


Figure S4. Statistical analysis of volume fraction of mineral deposits in the hydrogels gradients presented in Fig. 6b,c,e. The numbers in the margins of the figure indicate position in the gradient scaffolds. Grey squares indicate statistically significant differences ($p < 0.05$, ANOVA with Tukey's), whereas white squares indicate no statistical significance ($p > 0.05$).